Iranian Journal of Physics Research, Vol. 22, No. 3, 2022
DOI: 10.47176/ijpr.22.3.71276

Study of high spin phenomena in even-even dysprosium isotopes by using projected shell model

H Aghahasani, S Mohammadi, and Z Sajjadi
Department of Physics, Payame Noor University, PO BOX 19395-3697 Tehran, Iran

E-mail: mohammadi@pnu.ac.ir

(Received 2 July 2021 ; in final form 12 September 2022)

Abstract
Back-bending phenomenon which occurs at high spin states of some heavy mass nuclei has been studied, for the first time, by using the ratio of electromagnetic reduced transition probabilities B(M1)/B(E2) within the Projected Shell Model (PSM). In this model, all angular momenta are projected on the symmetry axis of the deformed nucleus, which makes shell model calculations much easier. The electric quadrupole transition probability B(E2) and the magnetic dipole transition probability B(M1) are sensitive to the nuclear shape deformation and nuclear charge distribution, respectively. As a result, any change in the nuclear rotation speed can change the transition probability ratios at high spins. Our ratio findings at high state spins in even - even 152-164Dy isotopes confirm the previous back-bendings seen in these isotopes, in good agreement wth the experimental data. Increasing spectroscopic quadrupole moments with spin is another high spin phenomenon in heavy mass nuclei studied in this paper. While intrinsic quadrupole moments are constant for each Dy isotope, this study shows that spectroscopic (observed) quadrupole moments are increasing with spin.

Keywords: projected shell model, high spins phenomena, dysprosium isotopes, electromagnetic reduced transition probability ratio, spectroscopic quadrupole moments

1. Introduction

High spin gamma-ray spectroscopy is one of the important tools in nuclear structure studies. The evolution of Yrast structure of neutron rich rare earth nuclei around the double mid shell had a lot of motivation to study these nuclei in recent years [1-18]. The gamma rays de-exciting the high spin states in rare earth nuclei were the subject of many studies in experimental and theoretical nuclear physics for several years. While there are different models for describing the nuclear structure, the most important one, that is the Nilsson model or the deformed shell model was presented in 1955 [2]. This model accurately expresses the splitting of energy-levels due to rotational motion of deformed (non-Spherical) nucleus. In 1995, the Projected Shell Model (PSM) was formulated as a deformed shell model projected on the nuclear symmetry axis by Hara and Sun [3], which was a sum of Nilsson deformed shell model and Bardeen-Cooper-Schrieffer (BCS) theory for considering the pairing effect between nucleons [4]. In the last two decades, this model has been used to explain a lot of high spin phenomena for heavy nuclei in rare earth nuclei. Double mid-shell nuclei with shell gaps between 50 to 82 for protons and 82 to 126 for neutrons in the lanthanide series have the largest number of valence particles and studies show that the quadrupole deformations are high in these nuclei. One of the tools to study shape changes in these nuclei is back bending phenomenon. This phenomenon occurs because the rotational energy of the nucleus exceeds the energy needed to break a pair of coupled nucleons. The unpaired nucleons then go into different orbits and increase the nuclear moment of inertia at some spins which cause reduction in nuclear rotation, so it looks like a back bending in the diagrams of moment of inertia J versus squared angular frequency ω^2 of the nucleus [5-14]. A new method to study the phenomenon of back bending is to use the ratio of reduced electromagnetic transition probabilities B(M1)/B(E2) versus spin. Even-even Dysprosium isotopes with Z=66 and N=86 to 98 are good candidates in the middle of lanthanide series to study these phenomena. Although back bending phenomena in Dy isotopes have been studied well in the past by drawing moment of inertia J versus squared

angular frequency ω^2 of the nucleus [10-13], in the present work systematic study of this phenomenon in even-even $^{152\text{-}154\text{-}156\text{-}158\text{-}160\text{-}162\text{-}164}$Dy isotopes have been done within PSM model by using changes of the ratio of electromagnetic transition probabilities $B(M1)/B(E2)$ versus spin. The same study has been done before for two isotopes of Erbium nuclei only [14]. Since the Er nuclei are at the end of lanthanide series, it was difficult to see the new effect in other isotopes.

Spectroscopic quadrupole moment (Q_s) is another important quantity to study at high spins within PSM model. We have intrinsic quadrupole moment (Q_0) and spectroscopic (observed) quadrupole moment (Q_s). The first one is defined in the intrinsic body-fixed frame of the nucleus and the second one in the laboratory frame. While there are no data for (Q_s) of other nuclei in the literature, we have studied this quantity for the first time for even-even Dy isotopes.

2. Projected shell model

The Spherical Shell Model (SSM) describes a nucleus as a system of independent fermions. In this model, each nucleon is assumed to move in an average field produced by the rest of nucleons [1]. As we go away from the shell closure, it was found that nuclei are deformed. To explain these deformed nuclei, the Nilsson model (deformed shell model) was introduced [2]. This is typically the first model used when examining data from deformed nuclei and calculates the total energy of a nucleus as a function of deformation.

Projected Shell Model (PSM) is another deformed version of spherical shell model approach where the potential is defined in the intrinsic frame of reference that breaks the rotational symmetry spontaneously. The main advantage of the PSM approach over Nilsson model is that it is plausible to perform a systematic analysis of high-spin band structures in a reasonable time frame with minimal computational effort [3].

In PSM approach the deformed basis is constructed by solving the deformed Nilsson potential with optimum quadrupole deformation parameters. The Nilsson basis states are then transformed to the quasiparticle space by using the simple BCS theory [4] for treating the pairing interaction to get the deformed quasiparticle basis.

As a result of Nilsson + BCS calculations, a set of qp states based on a vacuum qp state $|0\rangle$ in the intrinsic frame are constructed. The total Hamiltonian of the PSM model assumes the form [3],

$$\hat{H} = \hat{H}_0 + \frac{1}{2}\chi\sum \hat{Q}_\mu^+\hat{Q}_\mu - G_M\hat{P}^+\hat{P} - G_Q\sum \hat{P}_\mu^+\hat{P}_\mu, \qquad (1)$$

Here $\hat{H}_0$ is the deformed Woods-Saxon (or Harmonic Oscillator) single-particle Hamiltonian with the proper spin-orbit force. The deformed Woods-Saxon potential can be written as [3]:

$$V_N(r,\theta) = -\frac{V_0}{1+\exp\left[\dfrac{r - R_0 - R_T\varepsilon_2 Y_{20}(\theta) - R_T\varepsilon_4 Y_{40}(\theta)}{a}\right]}, \qquad (2)$$

where R_T is the target radius.

The second, third and fourth terms in equation (1) form the non-spherical Hamiltonian represent different kinds of characteristic correlations among active nucleons and consist of interaction terms quadrupole-quadrupole, monopole pairing and quadrupole pairing forces, respectively. The coefficients χ, G_M and G_Q are called the strengths of QQ + MP + QP interactions. The strength χ can be calculated self-consistently by using the quadrupole deformation parameter ε_2. All deformation parameters are chosen from Ref. [15]. The standard strength for the pairing interaction G_M is taken of the form

$$G_M = \left[20.12 \pm 13.13\frac{N-Z}{A}\right]A^{-1}(\text{MeV}), \qquad (3)$$

where "± " sign is for neutrons (protons). In the rare earth region, the strength of the quadrupole pairing G_Q is assumed to be proportional to G_M, $G_Q=\gamma G_M$, where the proportional constant γ is fixed as 0.16 [16]. After fixing the Hamiltonian, it is diagonalized within the shell model space spanned by a selected set of multi-quasiparticle states $|\Phi_k\rangle$. In PSM model, the list of quasiparticle states for even-even Dysprosium isotopes which consist of (0, 2 and 4) quasiparticles for an appropriate angular momentum I, are given by:

$$\left\{|\Phi_k\rangle\right\} = \left\{|0\rangle, a^+_{\upsilon_1}a^+_{\upsilon_2}|0\rangle, a^+_{\pi_1}a^+_{\pi_2}|0\rangle, a^+_{\upsilon_1}a^+_{\upsilon_2}a^+_{\pi_1}a^+_{\pi_2}|0\rangle\right\} \qquad (4)$$

where $|0\rangle$ is the vacuum state and a^+ are the quasi particle (qp) creation operators and the index $\nu(\pi)$ stands for neutrons (protons). An energy cutoff 2.5 MeV for a quasiparticle pair energy levels far away from the Fermi level has been introduced. More details of the PSM theory are given in Ref. [3].

3. Electromagnetic reduced transition probabilities

The evolution of the ground-state nuclear moments such as electric quadruple moment and magnetic dipole moment provide an indication of changes in the nuclear structure, especially of shell closures. While the first one is sensitive to nuclear shape changes, the second one is a sensitive probe to the nuclear charge distribution.

Not only the ground-state properties are useful indicators for the evolution of nuclear structure, but also excited nuclear states can be used to reveal the underlying shell structure. Reduced electromagnetic transition probabilities between the excited states are one of the most common measures for quadrupole collectivity and shape changes in nuclei. In general, the probability of an electric or magnetic transition of multipolarity λ is given by [17]:

$$B(\sigma\lambda, I_i \to I_f) = \frac{1}{2I_i+1}\left|\langle\Psi_f\|\hat{O}(\sigma\lambda)\|\Psi_i\rangle\right|^2, \qquad (5)$$

Table 1. Deformation parameters ε_2 and ε_4 used in the present calculation. The first theoretical and experimental Yrast 2+ energies

are also included.

Isotope (Z=66)	N (Neutrons)	ε_2 Quadrupole	ε_4 Hexadecapole	$(E_\gamma)_{th.}$ MeV	$(E_\gamma)_{ex.}$ MeV
152Dy	86	0.140	0.099	0.881	0.614
154Dy	88	0.192	0.030	0.281	0.334
156Dy	90	0.217	0.020	0.175	0.138
158Dy	92	0.242	0.027	0.120	0.099
160Dy	94	0.250	0.020	0.096	0.087
162Dy	96	0.258	0.007	0.084	0.081
164Dy	98	0.267	0.007	0.071	0.073

The reduced electric quadrupole B(E2) and magnetic dipole B(M1) transition probabilities from an initial state I_i to a final state I_f, can be expressed by the following equations [17]:

$$B(E2; I_i \to I_f) = \frac{e^2}{(2I_i+1)} \left| \langle I_f M_f | \hat{Q}_2 | I_i M_i \rangle \right|^2 , \quad (6)$$

$$B(M1; I_i \to I_f) = \frac{\mu^2{}_N}{(2I_i+1)} \left| \langle I_f M_f | \hat{M}_1 | I_i M_i \rangle \right|^2 , \quad (7)$$

$\hat{Q}_2$ and $\hat{M}_1$ are electric quadrupole and magnetic dipole operators, respectively. Finally, by considering the partial mean life time τ_p in each transition, the reduced transition probabilities B(E2) and B(M1) are given by [18-20]:

$$B(E2) = \frac{816}{E_\gamma^5 \tau_p} e^2 fm^4 MeV^5 ps , \quad (8)$$

$$B(M1) = \frac{56.8}{E_\gamma^3 \tau_p} \mu_N^2 MeV^3 fs , \quad (9)$$

And their ratio for every level becomes,

$$\frac{B(M1)}{B(E2)} \cong 7\times10^{-5} E_\gamma^2 \frac{\mu_N^2}{e^2 fm^4} \frac{1}{MeV^2} , \quad (10)$$

Which shows that their ratio is proportional to squared transition gamma energy $E^2\gamma$.

4. Electric quadruple moments

Electric quadrupole moments are other important quantities to describe in deformed nuclei. We have intrinsic quadrupole moment Q_0 and spectroscopic quadrupole moment Q_8. Intrinsic quadrupole moments are defined in the intrinsic body-fixed frame of the nucleus and are related to quadrupole deformation parameter ε_2 [21]:

$$Q_0 = \frac{3}{\sqrt{5\pi}} Z R_{av}^2 \varepsilon_2 (1 + 0.16\varepsilon_2) , \quad (11)$$

to second order in ε_2.

In the above relation, $R^2_{av}=(3/5)R^2_0 A^{⅔}$ and $R_0=1.2\,fm$. The spectroscopic (observed) quadrupole moments are defined in the laboratory frame and are related to the intrinsic quadrupole moments by the following relation [21]:

$$Q_s = Q_0 \left[\frac{3K^2 - I(I+1)}{(I+1)(2I+3)} \right], \quad (12)$$

where K is projection of the total angular momentum on the nuclear symmetry axis and I is total spin. The acceptable K values in this model are K=0 and K=2. The K=0 means that the deformation is aligned along the symmetry axis and therefore preserves axial symmetry. The K=2 mode represents a dynamic time dependent excursion from axial symmetry. The dependence of Q_s on K and spin I means that the shape of a rotating nucleus is different in intrinsic and laboratory frames. The time averaged shape of rotation of a prolate deformed nucleus ($\varepsilon_2>0$) about an axis perpendicular to the symmetry axis in intrinsic frame looks like a disc, or an oblate deformed nucleus in laboratory frame ($\varepsilon_2<0$) Considering nuclear symmetry axis in the PSM model, we choose K=0, so $Q_s \propto -Q_0$ always.

5. Results and discussion

The PSM configuration space generally includes 3 major harmonic shells for protons and neutrons. The calculations are done by considering three major shells N = 3, 4, 5 (N = 4, 5, 6) with an intruder orbital $h_{11/2}$ ($i_{13/2}$) for protons (neutrons). Nilsson parameters ε_2 (Quadrupole deformations) and ε_4 (Hexadecupole deformations) are chosen from Ref. [15] and are listed in table 1. Also, the first excited energy (E_γ) of the first Yrast level 2+ calculated by this model together with the experimental data are included in this table. As it can be seen from figure 1, by increasing neutron number N there is a decrease in 2+ first Yrast energy, while the quadrupole deformation increases.

Figure 2 shows back bending plots for Dy isotopes. This phenomenon occurs because the rotational energy of the nucleus exceeds the energy needed to break a pair of coupled nucleons. After breaking, the unpaired nucleons go into different orbits and increase the nuclear moment of inertia at some spins which cause reduction in nuclear rotation speed, so it looks like a back bending in the diagrams. The moment of inertia J is defined as $\{(4I-2)/(E(I)-E(I-2))\}\{\hbar^2/MeV\}$ and rotation speed ω as $(E(I)-E(I-2))/2$ [7,10,11,14,22]. All experimental data are taken from Ref. [23]. Our diagrams in figure 2 are a little different from diagrams of Velazquez, et al [10] due to different input data to PSM code. Also, more experimental data were available in this study for comparison with theoretical results. The data for ^{158}Dy were not included in figure 2 due to some irregularities in data.

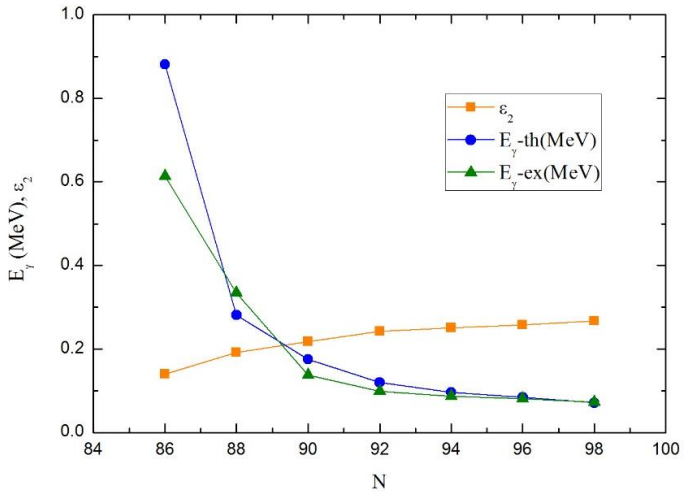

Figure 1. First excited energy E_γ of the first yrast level 2+ and Quadrupole deformation ε_2 versus neutron number N for $^{152\text{-}162}$Dy isotopes.

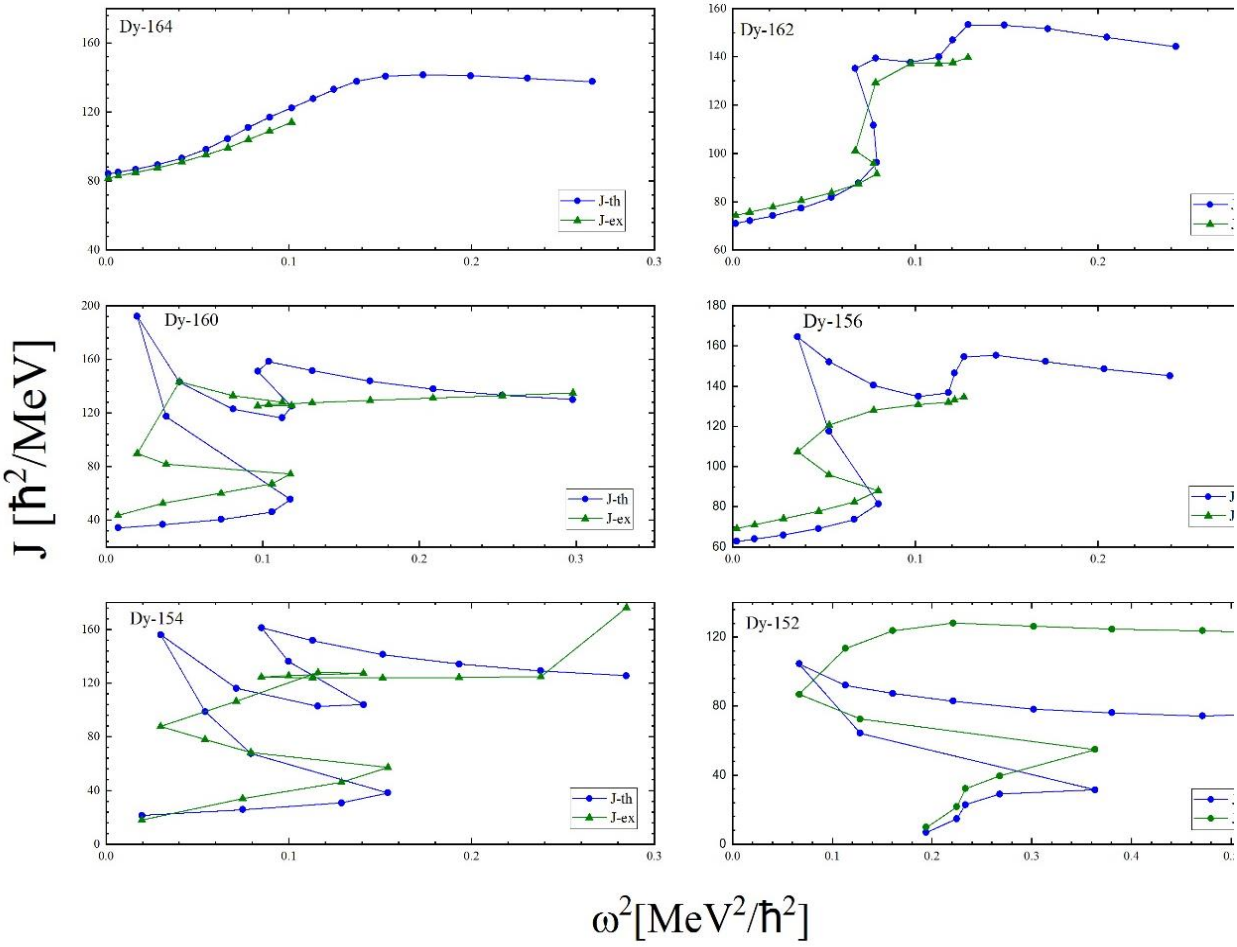

Figure 2. Back-bending plots for even-even Dy isotopes. Moments of inertia versus squared angular frequency. All data from tables 3 to 9.

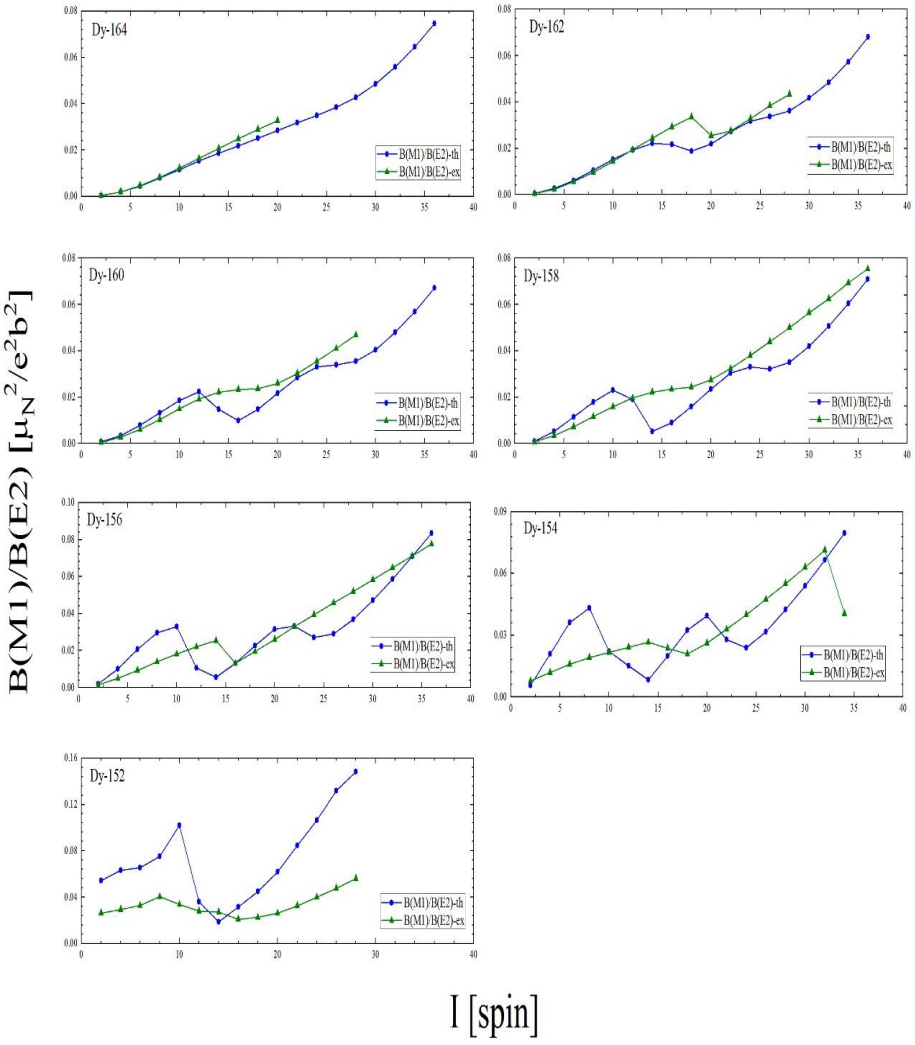

Figure 3. Electromagnetic reduced transition probabilities ratio B(M1)/B(E2) versus spin I for Dy isotopes. All data from tables 3 to 9.

As the electric quadrupole (E2) and the magnetic dipole (M1) moments are sensitive to nuclear shape deformation and nuclear charge distribution, respectively, any changes in the nuclear properties due to rotation, such as increasing in moment of inertia can change the transition probability ratio according to Eq. 10. Figure 3 shows electromagnetic reduced transition probabilities ratio B(M1)/B(E2) versus spin I for Dy isotopes. Again, all experimental data are taken from Ref. [23]. For ^{152}Dy, the electromagnetic transition ratio B(M1)/B(E2) increases gradually with increasing spin up to spin I=10$\hbar$ and suddenly drops at spin 14$\hbar$. This means that at first the dominant transitions in ^{152}Dy are mostly magnetic dipole transitions with a gradual increase in the contribution of the electric quadrupole transitions, as spin increases. This is the spin range where usual back bending phenomenon occurs in ^{152}Dy, as figure 2 shows. In other words, as nuclear moment of inertia increases due to alignment of $h_{9/2}$ 2qp-neutrons at spin I=10$\hbar$, the rotating speed suddenly decrease and this happens with a reduction in the dipole magnetic properties. For ^{154}Dy, the alignments of $h_{9/2}$ 2qp neutrons and $h_{11/2}$ 2qp protons at spins I=8$\hbar$ and 20$\hbar$, respectively, are related to two back bendings in this isotope, as figure 2 shows. The same trend happens for ^{156}Dy at spins I=10$\hbar$ and 22$\hbar$, for ^{158}Dy at spins I=10$\hbar$ and 24$\hbar$, for ^{160}Dy at spins I=12$\hbar$ and 24$\hbar$, and for ^{162}Dy at spins I=14$\hbar$ and 26$\hbar$. As it can been seen, by increasing neutron number, the back bending phenomena happen at higher spins which is related to more shape deformation in Dy isotopes. For ^{164}Dy isotope, since the last coupled neutrons are in $i_{13/2}$ intruder orbital, the back bending is hard to see. Tables 3 through 9 show all theoretical calculations and experimental data used in figures 2 and 3. All items in these tables have been defined in the text.

Table 2 shows intrinsic neutron and proton quadrupole moments Q_0 for Dy isotopes. Both quantities are constant in the intrinsic body-fixed frame of the nucleus. The polarization of closed proton shells by neutrons can be considered as inducing an effective charge on the neutron for quadrupole moments. Figure 4 shows that the ratio of intrinsic quadrupole moment of neutrons relative to protons are increasing with neutron number, which are related to excitation of neutrons to higher orbitals. In other words, the effective charge on neutrons are more prominent for higher orbitals.

Table 2. Calculated intrinsic neutron and proton quadrupole moments for Dy isotopes.

Isotope	Q_0 (neutrons)-barn	Q_0 (protons)-barn
152Dy	17.17	16.74
154Dy	23.83	22.56
156Dy	30.17	24.62
158Dy	36.51	26.24
160Dy	39.49	26.71
162Dy	42.21	27.12
164Dy	44.63	27.50

Table 3. Theoretical and experimental data for ^{152}Dy Isotope

I(Spin)	$\Delta E_{th.}$ MeV	$\omega^2_{th.}$ (frequency)	$J_{th.}$ (Inertia)	$\left[\frac{B(M1)}{B(E2)}\right]_{th.} = 0.07(\Delta E)^2_{th.}$	$\Delta E_{ex.}$ MeV	$J_{ex.} = \frac{4I-2}{\Delta E_{ex.}}$ (Inertia)	$\left[\frac{B(M1)}{B(E2)}\right]_{ex.} = 0.07(\Delta E)^2_{ex.}$
2	0.8812	0.1941	6.8092	0.0543	0.6138	9.7752	0.0263
4	0.9488	0.2250	14.7557	0.0630	0.6473	21.6283	0.0293
6	0.9665	0.2335	22.7626	0.0653	0.6834	32.1919	0.0326
8	1.0353	0.2680	28.9759	0.0750	0.7585	39.5517	0.0402
10	1.2062	0.3637	31.5033	0.1018	0.6930	54.8340	0.0336
12	0.7156	0.1280	64.2783	0.0358	0.6340	72.5552	0.0281
14	0.5165	0.0667	104.553	0.0186	0.6220	86.8167	0.0270
16	0.6730	0.1132	92.1295	0.0317	0.5470	113.3455	0.0209
18	0.8010	0.1604	87.3952	0.0449	0.5660	123.6749	0.0224
20	0.9408	0.2213	82.9060	0.0619	0.6090	128.0788	0.0259
22	1.0994	0.3022	78.2229	0.0846	0.6810	126.2848	0.0324
24	1.2336	0.3804	76.2026	0.1065	0.7540	124.6684	0.0397
26	1.3730	0.4713	74.2887	0.1319	0.8250	123.6363	0.0476
28	1.4545	0.5289	75.6273	0.1480	0.8950	122.9050	0.0560

Table 4. Theoretical and experimental data for ^{154}Dy Isotope

I(Spin)	$\Delta E_{th.}$ MeV	$\omega^2_{th.}$ (frequency)	$J_{th.}$ (Inertia)	$\left[\frac{B(M1)}{B(E2)}\right]_{th.} = 0.07(\Delta E)^2_{th.}$	$\Delta E_{ex.}$ MeV	$J_{ex.} = \frac{4I-2}{\Delta E_{ex.}}$ (Inertia)	$\left[\frac{B(M1)}{B(E2)}\right]_{ex.} = 0.07(\Delta E)^2_{ex.}$
2	0.2808	0.0197	21.3703	0.0055	0.3343	17.9479	0.0078
4	0.5466	0.0747	25.6152	0.0209	0.4122	33.9640	0.0118
6	0.7178	0.1288	30.6507	0.0360	0.4769	46.1312	0.0159
8	0.7853	0.1542	38.2003	0.0431	0.5235	57.3065	0.0191
10	0.5631	0.0793	67.4794	0.0221	0.5569	68.2348	0.0217
12	0.4654	0.0542	98.8323	0.0151	0.5885	78.1648	0.0242
14	0.3460	0.0299	156.058	0.0083	0.6161	87.6481	0.0265
16	0.5337	0.0712	116.169	0.0199	0.5816	106.602	0.0236
18	0.6809	0.1159	102.809	0.0324	0.5465	128.087	0.0209
20	0.7504	0.1408	103.949	0.0394	0.6124	127.367	0.0262
22	0.6321	0.0999	136.046	0.0279	0.6851	125.529	0.0328
24	0.5831	0.0850	161.219	0.0238	0.7558	124.3715	0.0399
26	0.6726	0.1131	151.641	0.0316	0.8230	123.9368	0.0474
28	0.7782	0.1514	141.358	0.0423	0.8870	124.0135	0.0550
30	0.8790	0.1932	134.243	0.0540	0.9492	124.3152	0.0630
32	0.9755	0.2379	129.160	0.0666	1.009	124.8761	0.0712
34	1.067	0.2847	125.562	0.0796	0.7609	176.1072	0.0405

Table 5. Theoretical and experimental data for ^{156}Dy Isotope

I(Spin)	$\Delta E_{th.}$ MeV	$\omega^2_{th.}$ (frequency)	$J_{th.}$ (Inertia)	$\left[\frac{B(M1)}{B(E2)}\right]_{th.} = 0.07(\Delta E)^2_{th.}$	$\Delta E_{ex.}$ MeV	$J_{ex.} = \frac{4I-2}{\Delta E_{ex.}}$ (Inertia)	$\left[\frac{B(M1)}{B(E2)}\right]_{ex.} = 0.07(\Delta E)^2_{ex.}$
2	0.1750	0.0077	34.2943	0.0021	0.1378	43.5413	0.0013
4	0.3810	0.0363	36.7425	0.0101	0.2663	52.5722	0.00496
6	0.5424	0.0735	40.5607	0.02059	0.3661	60.0928	0.00938
8	0.6509	0.1059	46.0868	0.02965	0.4452	67.3854	0.0138
10	0.6864	0.1178	55.3640	0.03298	0.5091	74.6415	0.01814
12	0.3920	0.0384	117.346	0.0107	0.5609	82.0110	0.02202
14	0.2813	0.0198	191.959	0.0055	0.6019	89.7158	0.02535
16	0.4332	0.0469	143.112	0.01313	0.4326	143.3194	0.01309
18	0.5697	0.0811	122.870	0.02271	0.5271	132.8021	0.01944
20	0.6707	0.1125	116.291	0.03148	0.6098	127.9107	0.02602
22	0.6882	0.1184	124.973	0.03315	0.6846	125.6208	0.03280
24	0.6225	0.0969	150.994	0.02712	0.7499	125.3500	0.03936
26	0.6442	0.1038	158.329	0.02904	0.8078	126.2688	0.04567
28	0.7256	0.1316	151.599	0.03685	0.8609	127.7732	0.05188
30	0.8213	0.1686	143.678	0.04721	0.9120	129.3859	0.0582
32	0.9139	0.2088	137.874	0.0584	0.9605	131.1816	0.0645
34	1.006	0.2530	133.195	0.0708	1.007	133.0685	0.0709
36	1.092	0.2980	130.054	0.0834	1.053	134.8528	0.0776

Table 6. Theoretical and experimental data for ^{158}Dy Isotope

I(Spin)	$\Delta E_{th.}$ MeV	$\omega^2_{th.}$ (frequency)	$J_{th.}$ (Inertia)	$\left[\frac{B(M1)}{B(E2)}\right]_{th.} = 0.07(\Delta E)^2_{th.}$	$\Delta E_{ex.}$ MeV	$J_{ex.} = \frac{4I-2}{\Delta E_{ex.}}$ (Inertia)	$\left[\frac{B(M1)}{B(E2)}\right]_{ex.} = 0.07(\Delta E)^2_{ex.}$
2	0.1200	0.0036	49.9908	0.0010	0.099	60.6060	0.0006
4	0.2711	0.0184	51.6442	0.0051	0.218	64.2201	0.0033
6	0.4026	0.0405	54.6464	0.0113	0.321	68.5358	0.0072
8	0.5063	0.0641	59.2591	0.0179	0.407	73.7100	0.0115
10	0.5721	0.0818	66.4237	0.0229	0.476	79.8319	0.0158
12	0.5216	0.0680	88.1848	0.0190	0.529	86.9565	0.0195
14	0.2707	0.0183	199.500	0.0051	0.563	95.9147	0.0221
16	0.3575	0.0320	173.412	0.0089	0.578	107.2664	0.0233
18	0.4746	0.0563	147.506	0.0157	0.590	118.6440	0.0243
20	0.5802	0.0842	134.429	0.0235	0.627	124.4019	0.0275
22	0.6596	0.1088	130.378	0.0304	0.679	126.6568	0.0322
24	0.6867	0.1179	136.888	0.0330	0.737	127.5440	0.0380
26	0.6776	0.1148	150.537	0.0321	0.793	128.6254	0.0440
28	0.7083	0.1254	155.308	0.0351	0.845	130.1775	0.0499
30	0.7746	0.1500	52.339	0.0420	0.898	131.4031	0.0564
32	0.8510	0.1811	148.057	0.0506	0.945	133.3333	0.0625
34	0.9289	0.2157	144.259	0.0603	0.995	134.6733	0.0693
36	1.007	0.2533	141.071	0.0709	1.037	136.9334	0.0752

Table 7. Theoretical and experimental data for ^{160}Dy Isotope

I(Spin)	$\Delta E_{th.}$ MeV	$\omega^2_{th.}$ (frequency)	$J_{th.}$ (Inertia)	$\left[\frac{B(M1)}{B(E2)}\right]_{th.} = 0.07(\Delta E)^2_{th.}$	$\Delta E_{ex.}$ MeV	$J_{ex.} = \frac{4I-2}{\Delta E_{ex.}}$ (Inertia)	$\left[\frac{B(M1)}{B(E2)}\right]_{ex.} = 0.07(\Delta E)^2_{ex.}$
2	0.0956	0.0023	62.7622	0.0006	0.0868	69.1244	0.0005
4	0.2191	0.0120	63.8863	0.0033	0.1968	71.1382	0.0027
6	0.3336	0.0278	65.9564	0.0077	0.2970	74.0740	0.0061
8	0.4342	0.0471	69.0904	0.0131	0.3855	77.8210	0.0104
10	0.5162	0.0666	73.6197	0.0186	0.4614	82.3580	0.0149
12	0.5649	0.0798	81.4265	0.0223	0.5226	88.0214	0.0191
14	0.4593	0.0527	117.580	0.0147	0.5633	95.8636	0.0222
16	0.3770	0.0355	164.454	0.0099	0.5765	107.5455	0.0232
18	0.4601	0.0529	152.157	0.0148	0.5805	120.5857	0.0235
20	0.5553	0.0771	140.476	0.0215	0.6086	128.1629	0.0259
22	0.6375	0.1016	134.908	0.0284	0.6572	130.8581	0.0302
24	0.6874	0.1181	136.751	0.0330	0.7117	132.0781	0.0354
26	0.6968	0.1214	146.394	0.0339	0.7652	133.2984	0.0409
28	0.7116	0.1266	154.585	0.0354	0.8178	134.5072	0.0468
30	0.7593	0.1441	155.406	0.0403	-	-	-
32	0.8275	0.1712	152.266	0.0479	-	-	-
34	0.9019	0.2034	148.571	0.0569	-	-	-
36	0.9785	0.2393	145.125	0.0670	-	-	-

Table 8. Theoretical and experimental data for ^{162}Dy Isotope

I(Spin)	$\Delta E_{th.}$ MeV	$\omega^2_{th.}$ (frequency)	$J_{th.}$ (Inertia)	$\left[\frac{B(M1)}{B(E2)}\right]_{th.} = 0.07(\Delta E)^2_{th.}$	$\Delta E_{ex.}$ MeV	$J_{ex.} = \frac{4I-2}{\Delta E_{ex.}}$ (Inertia)	$\left[\frac{B(M1)}{B(E2)}\right]_{ex.} = 0.07(\Delta E)^2_{ex.}$
2	0.0845	0.0018	71.0377	0.0004	0.0807	74.3494	0.0004
4	0.1940	0.0094	72.1646	0.0026	0.1849	75.7166	0.0023
6	0.2964	0.0220	74.2210	0.0061	0.2827	77.8210	0.0055
8	0.3881	0.0376	77.3080	0.0105	0.3725	80.5369	0.0097
10	0.4654	0.0541	81.6588	0.0151	0.4536	83.7742	0.0144
12	0.5247	0.0688	87.6661	0.0192	0.5262	87.4192	0.0193
14	0.5618	0.0789	96.1205	0.0220	0.5906	91.4324	0.0244
16	0.5552	0.0771	111.678	0.0215	0.6470	95.8268	0.0293
18	0.5181	0.0671	135.101	0.0187	0.6924	101.0976	0.0335
20	0.5596	0.0783	139.391	0.0219	0.6037	129.2032	0.0255
22	0.6243	0.0974	137.758	0.0272	0.6272	137.1173	0.0275
24	0.6718	0.1128	139.920	0.0315	0.6854	137.1461	0.0328
26	0.6943	0.1205	146.917	0.0337	0.7415	137.5590	0.0384
28	0.7178	0.1288	153.256	0.0360	0.7873	139.71802	0.0433
30	0.7711	0.1486	153.035	0.0416	-	-	-
32	0.8309	0.1726	151.638	0.0483	-	-	-
34	0.9054	0.2049	147.997	0.0573	-	-	-
36	0.9851	0.2426	144.145	0.0679	-	-	-

Table 9. Theoretical and experimental data for ^{164}Dy Isotope

I(Spin)	$\Delta E_{th.}$ MeV	$\omega^2_{th.}$ (frequency)	$J_{th.}$ (Inertia)	$\left[\frac{B(M1)}{B(E2)}\right]_{th.} = 0.07(\Delta E)^2_{th.}$	$\Delta E_{ex.}$ MeV	$J_{ex.} = \frac{4I-2}{\Delta E_{ex.}}$ (Inertia)	$\left[\frac{B(M1)}{B(E2)}\right]_{ex.} = 0.07(\Delta E)^2_{ex.}$
2	0.0713	0.0013	84.1800	0.0003	0.0734	81.7438	0.0003
4	0.1646	0.0068	85.0455	0.0018	0.1688	82.9383	0.0019
6	0.2537	0.0161	86.7093	0.0045	0.2591	84.9093	0.0046
8	0.3357	0.0282	89.3532	0.0078	0.3424	87.6168	0.0082
10	0.4077	0.0416	93.2045	0.0116	0.4176	90.9961	0.0122
12	0.4676	0.0547	98.3815	0.0153	0.4840	95.0413	0.0163
14	0.5163	0.0666	104.591	0.0186	0.5440	99.2647	0.0207
16	0.5584	0.0779	111.034	0.0218	0.5960	104.0268	0.0248
18	0.5984	0.0895	116.975	0.0250	0.6430	108.8646	0.0289
20	0.6373	0.1016	122.384	0.0284	0.6840	114.0350	0.0327
22	0.6734	0.1134	127.709	0.0317	-	-	-
24	0.7064	0.1247	133.073	0.0349	-	-	-
26	0.7406	0.1371	137.729	0.0383	-	-	-
28	0.7820	0.1529	140.656	0.0428	-	-	-
30	0.8334	0.1736	141.591	0.0486	-	-	-
32	0.8936	0.1996	141.008	0.0558	-	-	-
34	0.9603	0.2306	139.538	0.0645	-	-	-
36	1.0316	0.2661	137.644	0.0744	-	-	-

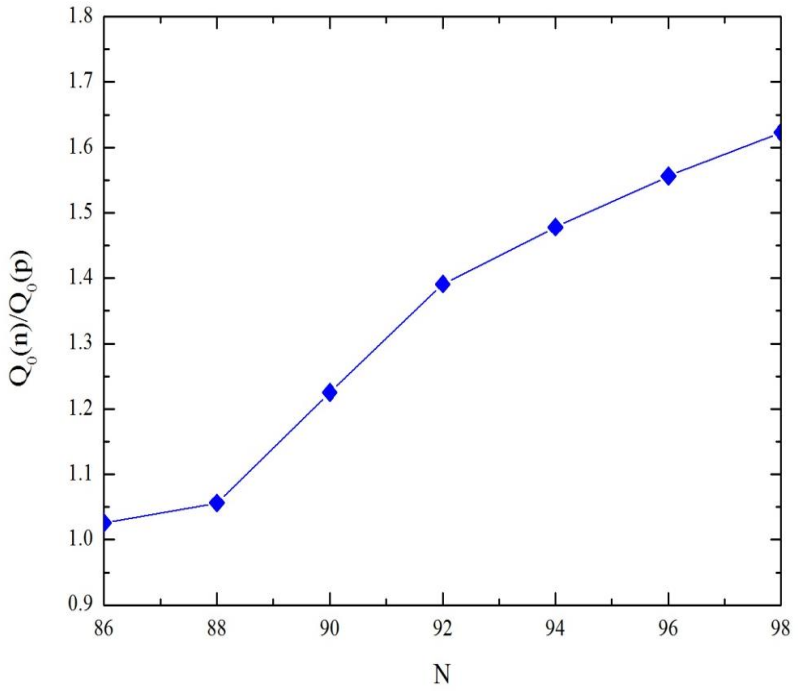

Figure 4. Intrinsic quadrupole moment ratio of neutrons relative to protons versus neutron number

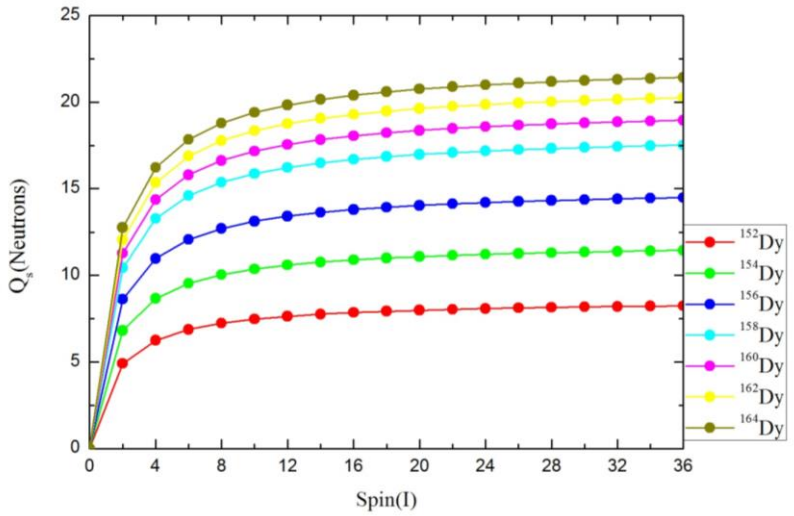

Figure 5. Neutron spectroscopic or observed quadrupole moments versus spin I for Dy isotopes.

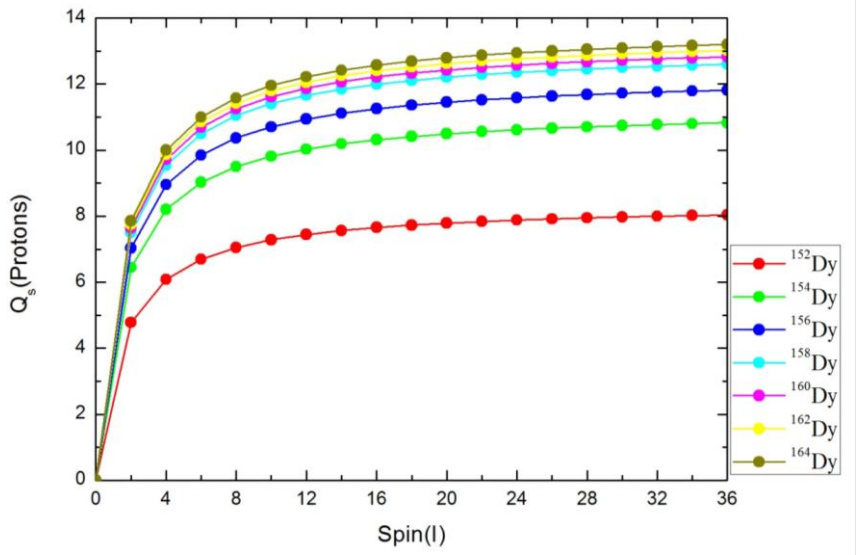

Figure 6. Proton spectroscopic or observed quadrupole moments versus spin I for Dy isotopes.

But as figures 5 and 6 show, the spectroscopic or observed quadrupole moments Q_s which are defined in the laboratory frame, are increasing with spin for both neutrons and protons. This increase which is related to quadrupole shape changes is again more prominent for neutrons than protons for heavier isotopes and again is related to excitation of neutrons to higher orbitals. Due to unavailability of experimental data for the spectroscopic quadrupole moments of even-even Dy isotopes, no comparison could be done.

6. Conclusions

In this paper, two high spin phenomena have been studied for Dy isotopes by using the projected shell model (PSM). Back-bending phenomena for even-even $^{152\text{-}164}$Dy isotopes have been studied for the first time by using the ratio of electromagnetic reduced transition probabilities B(M1)/B(E2) up to spin 36$\hbar$ and compared with available experimental data. These new findings confirm the well-known back bendings seen before by drawing moment of inertia J versus squared angular frequency ω^2 of the nucleus. This phenomenon occurs because the rotational energy of the nucleus exceeds the energy needed to break a pair of coupled nucleons. The unpaired nucleons then go into different orbits and increase the nuclear moment of inertia at some spins which cause reduction in nuclear rotation, so it looks like a back bending in the diagrams. For each Dy isotope, the electromagnetic transition ratio B(M1)/B(E2) increases gradually with increasing spin and suddenly drops at some higher spins. This is the spin range which usual back-bending phenomenon (change of moment of inertia J versus squared angular frequency ω^2) occurs in these isotopes. In other words, the back-bending phenomenon which is related to the breaking of nucleon pairs and their alignments with nuclear core rotation has been observed also as changes in the ratio of electromagnetic reduced transition probabilities versus spin as shown in figure 3.

The intrinsic quadrupole moment ratio of neutrons relative to protons $Q_0(n)/Q_0(p)$ is increasing versus neutron number, which means the effective charge on

neutrons are more prominent for heavier isotopes. The polarization of closed proton shells by neutrons can be considered as inducing an effective charge on the neutrons for quadrupole moments. Increasing spectroscopic (observed) quadrupole moments Q_s with spin is another high spin phenomenon in heavy mass nuclei studied in this model. These moments which are defined in the laboratory frame, are also increasing with spin for both neutrons and protons which are more prominent for neutrons than protons for heavier isotopes. This phenomenon is related to occupying higher orbitals and hence more polarization of closed proton shells by excited neutrons.

Acknowledgment
We are most grateful to our colleagues Dr F. Fadaei and Dr N. Shayan Shakib for kindly reading and carefully checking this manuscript.

References

1. A Bohr and B Mottelson,*"Nuclear structure*" World Scinetific (1998).
2. S G Nilsson, *Math. Phys. Medd.* **29** (1955) 16.
3. K Hara and Y Sun, *Intern. J. Mod. Physics* E **4**, 4 (1995) 637.
4. Y Sun and K Hara, *Comp. Phys. Commun* **104** (1997) 245.
5. J Bardeen, L N Cooper, and J R Schrieffer *Phys. Rev.* **108** (1957) 1175.
6. B Slathia, R Devi, and S K Khosa, *Nucl. Phys* A **943** (2015) 39.
7. T Shizuma, *et al*., *Phys. Rev.* C **69** (2004) 024305.
8. P Verma, *et al., Nucl. Phys.* A **918** (2013) 1
9. G Krishan, *et al., Pram. J. of Phys.* **83** (2014) 341.
10. B Slathia, R Devi, and S K Khosa, *Indi. J. phys.* **90** (2016) 1165.
11. V Velaquez, *et al., Nucl. Phys.* A **653** (1999) 355.
12. Z Wen Hua and G Jian Zhong, *Chin. Phys. Lett.* **27**, 1 (2010) 012101.
13. Y Sun and J L Egido, *Nucl. Phys.* A **580** (1994) 1.
14. A N Behkami and M N Nasrabadi, *Commun. Theor. Phys.* **37**, 4 (2002) 47.
15. M Shahriarie, S Mohammadi, and Z Firouzi, *J. Korean Phys. Soc.* **76** (2020) 8.
16. P Möller, *et al*., *At. Data Nucl. Data Tables* **109** (2016) 1.
17. J A Sheikh, Y Sun, and P M Walker, *Phys. Rev.* C **57** (1998) R26.
18. J Suhonen,"*Electromagnetic Multipole Moments and Transitions*" Springer, Berlin, Heidelberg (2007).
19. D Ram, R Devi, and S Khosa, *Pramana J. Phys.* **80** (2013) 953.
20. B Castel and I S Towner, "*Modern theories of nuclear moments*", Clarendon Press (1990).
21. B A Brown, "*Lecture notes in nuclear structure physics, National Super Conducting Cyclotron Laboratory*" Michigan State University (2005).
22. R F Casten, "*Nuclear Structure from a Simple Perspective"* Oxford University Press (2000).
23. K S K Krane, "*Introductory Nuclear Physics*", John Wiley and Sons (1987).
24. D Radware, *MS Thesis,* McGill University (2020).